JPE 17-3-19

https://doi.org/10.6113/JPE.2017.17.3.766
ISSN(Print): 1598-2092 / ISSN(Online): 2093-4718

Comparison of Dynamic Characteristics between Virtual Synchronous Machines Adopting Different Active Power Droop Controls

Chang Yuan†, Chang Liu*, Xueyin Zhang*, Tianyang Zhao*, Xiangning Xiao*, and Niang Tang**

†,*State Key Laboratory of Alternate Electrical Power System with Renewable Energy Sources, North China Electric Power University, Beijing, China
** Electric Power Research Institute of Guangdong Power Grid Co., Ltd., Guangzhou, China

Abstract

In modern power systems, high penetration of distributed generators (DGs) results in high stress on system stability. Apart from the intermittent nature of DGs, most DGs do not contribute inertia or damping to systems. As a result, a new control method named virtual synchronous machine (VSM) was proposed, which brought new characteristics to inverters such as synchronous machines (SMs). In addition, different active power droop controls for VSMs are being proposed in literatures. However, they are quite different in terms of their dynamic characteristics despite of the similar control laws. In this paper, mathematical models of a VSM adopting different active power droop controls are built and analyzed. The dynamic performance of the VSM output active power and virtual rotor angular frequency are presented for different models. The influences of the damping factor and droop coefficient on the VSM dynamic behaviors are also investigated in detail. Finally, the theoretical analysis is verified by simulations and experimental results.

Key words: Active power control, Damping factor, Droop control, Dynamic characteristics, Virtual synchronous machine (VSM)

I. INTRODUCTION

In order to solve environmental problems and energy crisis, distributed generators (DGs) have been quickly developed in recent years. According to the data from the Chinese government, the installed capacities of wind and solar power in China reached 129GW and 43.18GW at the end of 2015 [1], [2]. China has become the largest country in terms of solar power installed capacity in the world and wind power corresponds to 8.6% of chinese electricity generation capacity [1], [2]. In Europe, USA, Japan and India, significant targets are also being considered for the use of DGs and renewable energy sources in their power systems in the next two decades [3].

DGs employing grid connected power electronic converters results in high stress on power system frequency stability. Apart from their intermittent nature, most DGs do not contribute inertia and damping to systems. The inertia and damping in traditional power systems mainly come from synchronous machines. However, the equivalent rotating inertia and damping in current power system keep decreasing due to replacing synchronous generators with DGs. Wind turbines have kinetic energy, stored in their blades, gear box and generator. However, they cannot directly support power system. PV units do not have any equivalent rotating parts which can be used as an energy buffer to deliver inertia to the system except for the energy stored in their capacitors [4], [5].

Virtual synchronous machines (VSMs) have become a promising method to solve frequency stability problems. The inverters employing VSM control can operate like synchronous generators to provide inertia and damping to power systems. The first proposal of a "Virtual Synchronous Machine", was published by Beck and Hesse in 2007[6]. Since then, VSMs have been investigated in [3], [5]-[28] in recent years.

Manuscript received Sep., 22, 2016; accepted Feb. 6, 2017
Recommended for publication by Associate Editor Kai Sun.
†Corresponding Author: yc_ncepu@163.com
Tel: +86-13810185866, North China Electric Power University
*State Key Lab. of Alternate Electrical Power System with Renewable Energy Sources, North China Electric Power Univ., China
**Electric Power Research Inst. of Guangdong Power Grid Co., Ltd., China

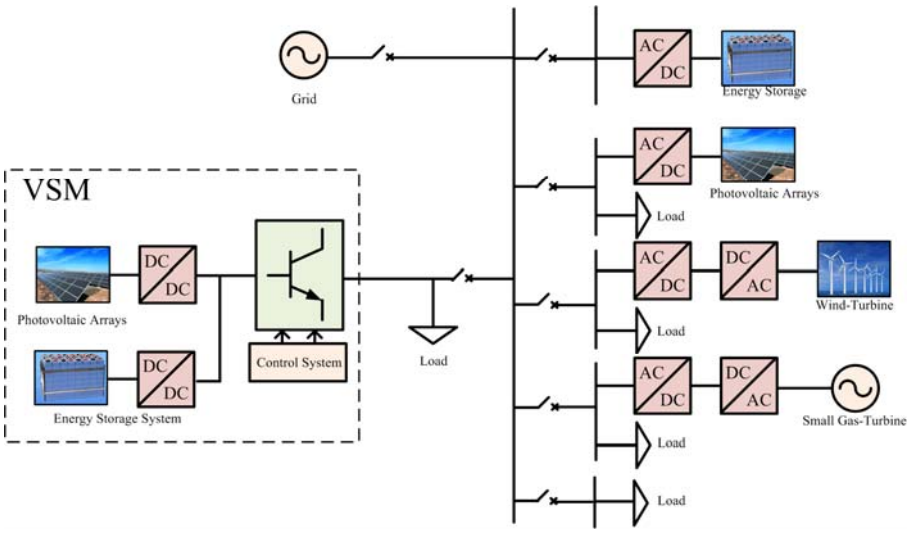

Fig. 1. A typical micro-grid with a VSM.

Energy storage is one of the most important parts for VSMs to provide inertia and damping to systems. When a disturbance occurs, the rotating masses inject or absorb energy into or from the grid to counteract the frequency deviation in conventional power system with synchronous generators. This phenomena can be mimicked by an energy storage system (ESS) through proper discharging or charging control [7]-[9].

There are different methods for VSM active power control. The swing equation in equation (1) was introduced in [10]-[14] for the grid-connected mode.

$$\begin{cases} 2H\dfrac{d\omega^*}{dt} = P_m^* - P_e^* - D(\omega^* - 1) \\ \dfrac{d\delta}{dt} = \omega_0(\omega^* - 1) \end{cases} \tag{1}$$

where P_m is the virtual shaft power determined by the governor, P_e is the measured output active power, H is the virtual inertia constant, D is the virtual damping factor, ω is the virtual rotor angular frequency, 1 is the nominal angular frequency ω_0 in per unit (p.u.), and * suggests that the parameter is in p.u..

The droop control in the governor can be written as

$$P_m^* - P_{ref}^* = \frac{1}{K}(1 - \omega^*) \tag{2}$$

where P_{ref} is the reference of the output active power, and K is the droop coefficient.

Equation (3) can be obtained from (1) and (2).

$$2H\frac{d\omega^*}{dt} = P_{ref}^* + (\frac{1}{K} + D)(1 - \omega^*) - P_e^* \tag{3}$$

From the analysis in [17]-[19] and equation (3), the damping factor is equivalent to the droop coefficient in this mode.

The swing equation (4) is used in [20]-[28] for a VSM in the micro-grid connected mode. Equations (5) and (6) for different droop control methods have been adopted in the literature.

$$\begin{cases} 2H\dfrac{d\omega^*}{dt} = P_m^* - P_e^* - D(\omega^* - \omega_g^*) \\ \dfrac{d\delta}{dt} = \omega_0(\omega^* - \omega_g^*) \end{cases} \tag{4}$$

where ω_g is the micro-grid frequency.

Equation (5), for the droop control method, is adopted in [20]-[21].

$$P_m^* - P_{ref}^* = \frac{1}{K}(\omega_{ref}^* - \omega_g^*) \tag{5}$$

where ω_{ref} is the reference frequency, and is usually equal to ω_0.

Equation (6) for the droop control method is adopted in [22]-[28].

$$P_m^* - P_{ref}^* = \frac{1}{K}(\omega_{ref}^* - \omega^*) \tag{6}$$

There are large differences in the dynamic characteristics based on these similar equations (2), (5) and (6). Firstly,the damping factor and droop coefficient K are no longer equivalent using equation (4)-(6) when compared with equation (1) and (2). Secondly, equations (5) and (6) for droop control have different impacts on the dynamic behaviors of a VSM.

Different models for VSMs were listed in [22], and different droop controls were applied in the analysis. The relations between the damping factor D and the droop coefficient K have been discussed. However, the influences of different droop control methods on VSM dynamic behaviors have not been discussed in the literature.

This paper is organized as follows. In section II, the operating principle of a VSM is presented. A comparison of different VSM mathematical models is studied in detail in section III. A theoretical analysis of the VSM characteristics is investigated in section IV. The control method and simulation results are presented in sections V and VI,

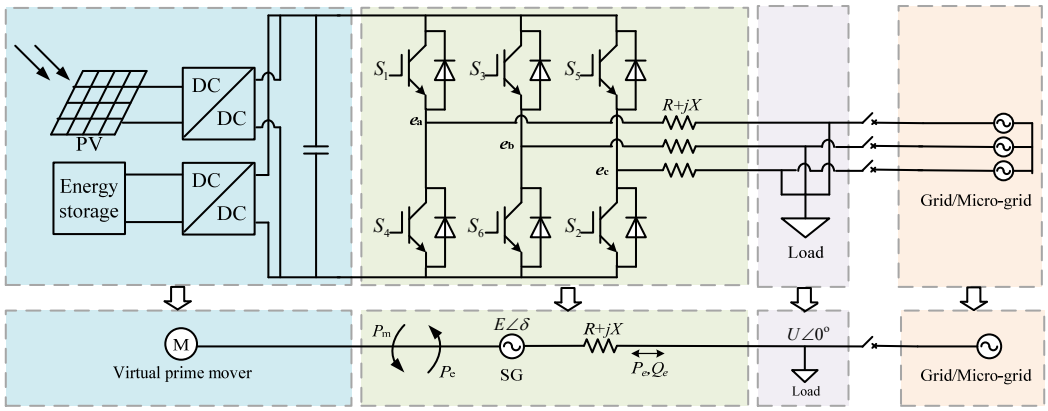

Fig. 2. Corresponding relations between a VSM and a SM.

respectively. Experiment results are presented in section VII. Finally, some conclusions are presented in section VIII.

II. Operating Principle of a VSM

A typical system structure of a VSM is shown in Fig. 1, including a small gas turbine, wind turbines, photovoltaic arrays, energy storage and loads. These sources are connected to a point of common coupling (PCC) via a switch, and they contain two operation modes. Inverters employing VSM control can provide inertia and damping to systems, and to mitigate the frequency variation process.

The VSM in Fig. 1 contains PVs, energy storage and an inverter employing VSM control. The corresponding relations between the VSM and the synchronous machine(SM) are shown in Fig. 2. The essential part of the VSM and SM can be equivalent as follows. The PV can be considered to be a prime mover and the ESS can be considered to be a rotating part of the prime mover and generator. The electromechanical energy conversion process can be realized by an inverter employing VSM control.

III. Modeling of a VSM

According to the references, different droop control models of VSM are listed in the following. The differences between these models for the micro grid-connected mode are also analyzed.

Equation (7) can be obtained according to equation (4) and is written as

$$\begin{cases} 2Hs\Delta\omega^*(s)=\Delta P_m^*(s)-\Delta P_e^*(s)-D(\Delta\omega^*(s)-\Delta\omega_g^*(s)) \\ s\Delta\delta(s)=\omega_0(\Delta\omega^*(s)-\Delta\omega_g^*(s)) \end{cases} \tag{7}$$

Equation (8) can be obtained from equation (5) and is written as:

$$\Delta P_m^*(s)=-\frac{1}{K}\Delta\omega_g^*(s) \tag{8}$$

The output resistance and inductance are taken into consideration. The output current of a VSM can be derived from Kirchhoff's law, and is written as:

$$\dot{I}=\frac{E\angle\delta-U}{Z\angle\alpha} \tag{9}$$

where E is the potential of the VSM, and U is the VSM terminal voltage. The impedance $Z=((\omega L)^2+R^2)^{1/2}$. R and L are the line resistance and inductance, respectively.

The output apparent power of the VSM can be conducted as follows:

$$\begin{aligned} S_{VSM}&=U\bar{\dot{I}} \\ &=\frac{EU\angle(-\delta)-U^2}{Z\angle(-\alpha)} \\ &=\frac{EU}{Z}\cos(\alpha-\delta)+j\frac{EU}{Z}\sin(\alpha-\delta)-\frac{U^2}{Z}\cos\alpha-j\frac{U^2}{Z}\sin\alpha \\ &=P_e+jQ_e \end{aligned} \tag{10}$$

where the superscript "-" indicates the conjugate operation of the element, and the impedance angle $\alpha=\tan^{-1}(\omega L/R)$. P_e is the output active power of the VSM. Q_e is the output reactive power of VSM. It can be concluded from equatio0 n(10) that:

$$\begin{cases} P_e=EU\cos(\alpha-\delta)/Z-U^2\cos\alpha/Z \\ Q_e=EU\sin(\alpha-\delta)/Z-U^2\sin\alpha/Z \end{cases} \tag{11}$$

E_s and δ_s can be calculated when $P_e=P_{ref}$ and $Q=Q_{ref}$,where E_s is the potential of the VSM, and δ_s is the power angle in the steady state.

$$\begin{cases} \delta_s=\alpha-\tan^{-1}\left(\dfrac{Q_{ref}+U^2\sin\alpha/Z}{P_{ref}+U^2\cos\alpha/Z}\right) \\ E_s=\dfrac{Q_{ref}Z+U^2\sin\alpha}{U\sin(\alpha-\delta_s)} \end{cases} \tag{12}$$

The mathematical model of P_e^* can be deduced from (11).

$$\Delta P_e^*=\frac{EU}{S_nZ}[\cos(\alpha-\delta-\Delta\delta)-\cos(\alpha-\delta)] \tag{13}$$

where S_n is the rated apparent power of the VSM.

When $\Delta\delta\to0$, $\cos(\Delta\delta)\to1$, $\sin(\Delta\delta)\to\Delta\delta$, equation (13) can be simplified as

$$\Delta P_e^*=\frac{EU}{S_nZ}\sin(\alpha-\delta)\Delta\delta \tag{14}$$

Equation (15) can be obtained by a Laplace transform of

(14).

$$\Delta P_e^*(s) = \frac{EU}{S_n Z}\sin(\alpha-\delta)\Delta\delta(s) \tag{15}$$

Let S_E=EUsin(α-δ)/$S_n Z$, which is the synchronizing power coefficient. According to equation (12), it can be written as

$$S_E = Q_{ref}^* + \frac{U^2\sin\alpha}{ZS_n} \tag{16}$$

It can be summarized that S_E is related to Q_{ref} instead of P_{ref}.

The transfer functions in (17) and (18) of ΔP_e^* to ΔP_{ref}^* can be concluded from equations (4)-(6) and (14). Equation (17) and (18) are the transfer functions derivated for (5) and (6), respectively.

$$\frac{\Delta P_e^*(s)}{\Delta P_{ref}^*(s)} = \frac{\omega_0 S_E}{2Hs^2 + Ds + \omega_0 S_E} \tag{17}$$

$$\frac{\Delta P_e^*(s)}{\Delta P_{ref}^*(s)} = \frac{\omega_0 S_E}{2Hs^2 + (D+\frac{1}{K})s + \omega_0 S_E} \tag{18}$$

The transfer functions of $\Delta\omega_g^*$ to ΔP_e^* and $\Delta\omega_g^*$ to $\Delta\omega^*$ can be concluded from equations (7), (8) and (15) so that:

$$\frac{\Delta P_e^*(s)}{\Delta\omega_g^*(s)} = -\frac{(2Hs+1/K)\omega_0 S_E}{2Hs^2 + Ds + \omega_0 S_E} \tag{19}$$

$$\frac{\Delta\omega^*(s)}{\Delta\omega_g^*(s)} = \frac{(D-1/K)s + \omega_0 S_E}{2Hs^2 + Ds + \omega_0 S_E} \tag{20}$$

The transfer functions of $\Delta\omega_g^*$ to ΔP_e^* and $\Delta\omega_g^*$ to $\Delta\omega^*$ when the droop control is represented by equation (6) can be conducted in the same way. Therefore:

$$\frac{\Delta P_e^*(s)}{\Delta\omega_g^*(s)} = -\frac{(2Hs+1/K)\omega_0 S_E}{2Hs^2 + (D+1/K)s + \omega_0 S_E} \tag{21}$$

$$\frac{\Delta\omega^*(s)}{\Delta\omega_g^*(s)} = \frac{Ds + \omega_0 S_E}{2Hs^2 + (D+1/K)s + \omega_0 S_E} \tag{22}$$

According to the types of poles of equations (19)-(22), the system state can be divided into three modes. They include the under damping mode for two conjugate complex poles, the over damping mode for two unequal negative real poles and the critical damping mode for two equal negative real poles.

IV. Theoretical Analysis of the System Characteristics of a VSM.

In this section, the influences of K and D on the VSM dynamic behavior are analyzed. Bode diagrams and pole trajectories are also presented. The parameters of the system with the VSM are shown in Table I. When Q_{ref}=0 kVar and H=0.05s, S_E can be calculated as 1.038 by equation (16). D=5 is designed for the under damping mode and D=14 is designed for the over damping mode according to the analysis in Section III.

TABLE I
Parameter of a VSM System

Parameter	Value	Parameter	Value
S_n	250kVA	P_{ref}	10kW
U_g(L-L)	380V	U_{dc}	800V
L	1.5mH	ω_{ref}	314rad/s
R	0.2Ω	$\Delta\omega_g^*$	0.01
H	0.05s	K	0.05

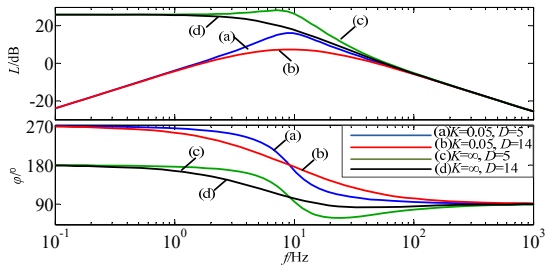

(a) Transfer function in equation (19).

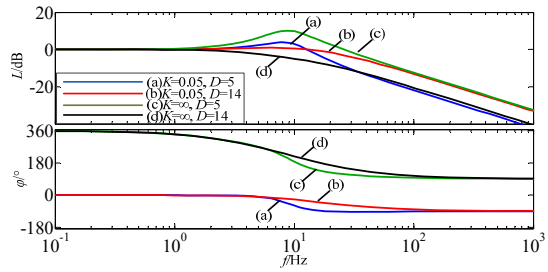

(b) Transfer function in equation (20).

Fig. 3. Bode diagrams with different K and D.

A. Comparison between the Damping Factor and the Droop Coefficient

The bode diagrams in Fig. 3(a) are obtained from equation (19), and those of Fig. 3(b) are obtained from equation (20).

According to the magnitude-frequency characteristic in Fig. 3(a), a smaller damping factor D has a greater impact on the magnitude characteristic of the transfer function. In addition, K makes the characteristic curve move up. From the phase-frequency characteristic in Fig. 3(a), the phase margin increases by the increase of D. In addition, K contributes to an increase of the phase margin.

According to the magnitude-frequency characteristic in Fig. 3(b), a smaller damping factor D has a greater impact on the magnitude characteristic of the transfer function. From the phase-frequency characteristic Fig. 3(b), the phase margin increases by an increase of D. In addition, K contributes to a decrease of the phase margin.

The droop coefficient K has a different effect on the output active power and rotor angular frequency in the magnitude-frequency characteristic and phase-frequency characteristic. An increase of the damping factor D can enhance system stability.

The droop coefficient has been shown to be similar to the

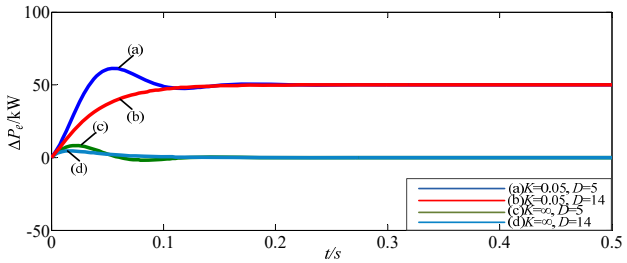

(a) Output active power with different values of K and D.

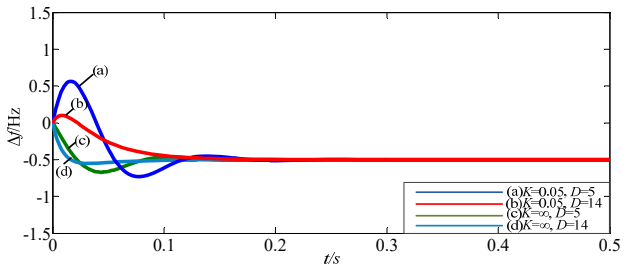

(b) Virtual rotor frequency with different values of K and D.

Fig. 4. Dynamic responses of the output active power and virtual rotor frequency when the micro-grid frequency steps.

damping factor in some papers. However, when ω_0 is changed to the measured parameter ω_g, the droop coefficient is no longer equivalent to the damping factor. The dynamic behaviors of the output active power ΔP_e and the virtual rotor frequency Δf are shown in Fig. 4 when the micro-grid frequency steps down by 1%. There is no output active power in Fig. 4(a), at last while K is infinite when compared to K=0.05. In addition, Δf tends to be equal to Δf_g in Fig. 4(b).Therefore, it can be concluded that damping factor D has no influence on the steady value for Δf-Δf_g=0.

It can also be concluded from Fig. 4 that damping factor D has no influence on the steady value of ΔP_e. However, it influences the transient value of ΔP_e. The droop coefficient K influences both the steady value and transient value of ΔP_e.

From Fig. 4(b), both D and K influence the transient value of the virtual rotor frequency. However, its steady value is not influenced by D and K.

B. Comparison between Different Droop Control Methods

The bode diagrams in Fig. 5(a) and (b) are obtained from equation (19) and (21), and those in Fig. 5(c) and (d) are obtained from equation (20) and (22). The symbols in the legend are represented by ω_g and ω. They represent the different droop control methods in equations (5) and (6), respectively.

According to the magnitude-frequency characteristic in Fig. 5(a) and (b), there is no overshoot in equation (6). From the phase-frequency characteristic in Fig. 5(a) and (b), the phase margin of equation (5) is larger than equation (6).

According to the magnitude-frequency characteristic in Fig. 5(c) and (d), there is no overshoot in equation (6). From the phase-frequency characteristic in Fig. 5(c) and (d), the phase margin of equation (5) was larger than equation (6).

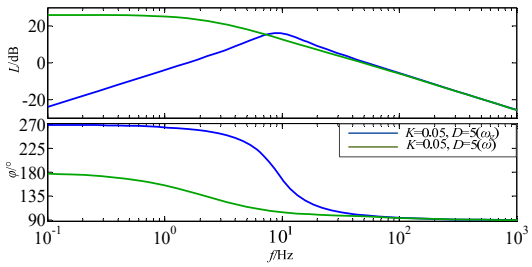

(a) Transfer functions in equations (19) and (21).

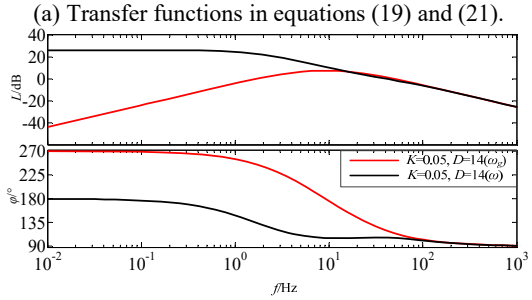

(b) Transfer functions in equations (19) and (21).

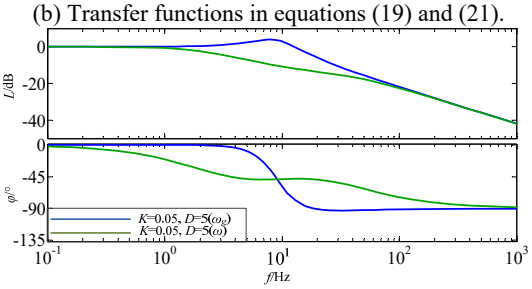

(c) Transfer functions in equations (20) and (22).

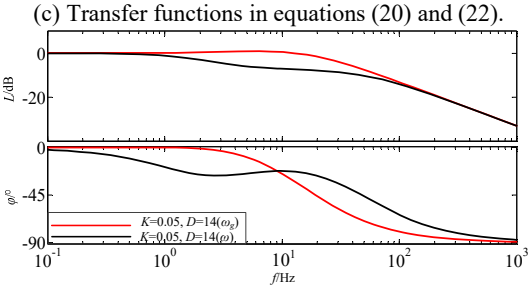

(d) Transfer functions in equations (20) and (22).

Fig. 5. Bode diagrams with different droop control methods.

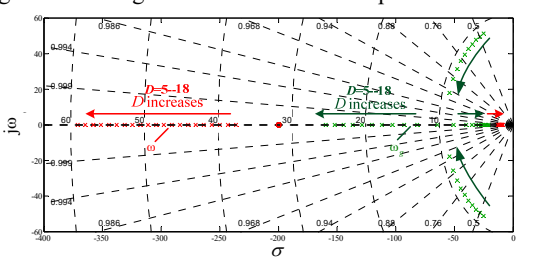

(a) Transfer functions in equations (19) and (21).

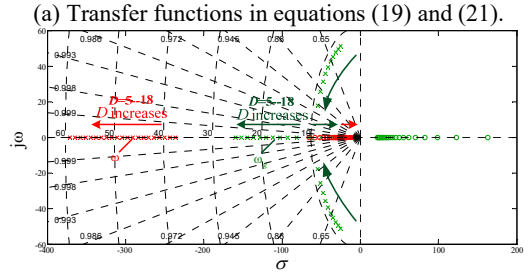

(b) Transfer functions in equations (20) and (22).

Fig. 6. Pole and zero point trajectories with different droop control methods.

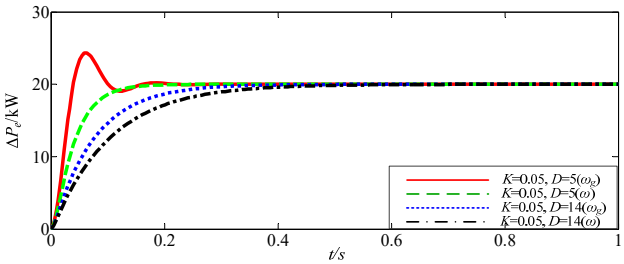

Fig. 7 Dynamic responses of the output active power when P_{ref} steps with different droop control methods.

Pole and zero point trajectories with the two different droop control methods are shown in Fig. 6. They are obtained from equations (19)-(22) when H=0.05s and D varies from 5 to 18. Equation (5) transfers from the under damping mode to the over damping mode when the damping factor D varies. However, only equation (6) involves two unequal negative real poles and is located in the over damping mode because the droop coefficient increases the damping of the VSM.

1) Reference of the Output Active Power Rises: The dynamic responses of the output active power when P_{ref} steps from zero to 20kW with different droop control methods are shown in Fig. 7 according to the transfer functions in equations (17) and (18). It can be concluded that the droop control method employing equation (6) can significantly increase system damping when compared with equation (5).

2) Micro-Grid Frequency Drops: The dynamic responses of the VSM when the micro-grid frequency steps with different droop control methods are shown in Fig. 8 and Fig. 9. The responses of the output active power are shown in Fig. 8, and the results show that the droop control method in equation (6) can increase the damping of the VSM. The responses of virtual rotor frequency are shown in Fig. 9, and it can be concluded that the droop control employing equation (6) can significantly increase the system damping when compared with equation (5). However, the response of the virtual rotor frequency with equation (5) in Fig. 9(b) is not located in the over damping mode when compared with the output active power in Fig. 8(b). The transfer function in equation (20) obtains the positive zero point when D<1/K.

V. CONTROL SYSTEM

A control diagram of a VSM is presented in this section. The control system mainly includes an active power control and a reactive power control. A control diagram and the main circuit involved in simulations are shown in Fig. 10. The active power control is designed according to the swing equation in equation (4). The relationship between the rotor angle φ and the power angle δ can be written as equation (23). The reactive power control is designed based on the error between the reference and measured value through a PI controller. In addition, the modulation signal E is the sum of ΔE_Q and the phase voltage effective value of the grid. The

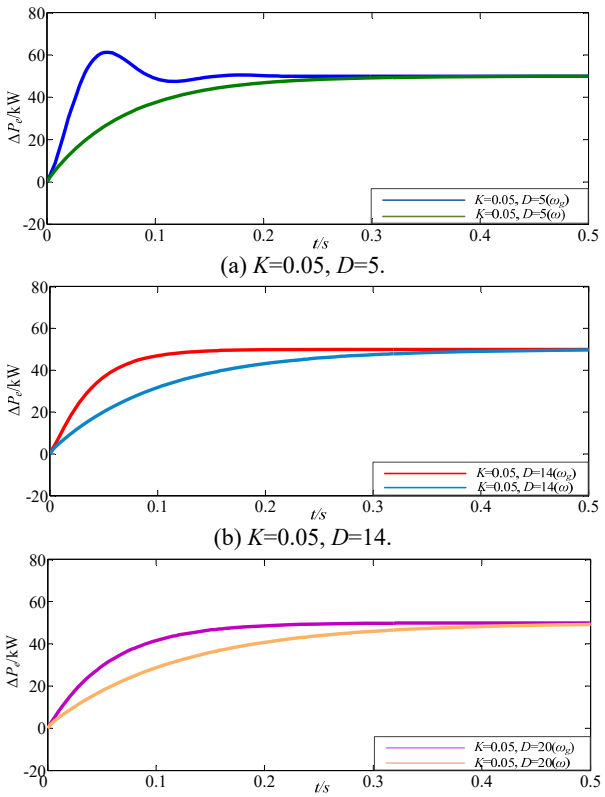

(a) K=0.05, D=5.

(b) K=0.05, D=14.

(c) K=0.05, D=20.

Fig. 8. Dynamic responses of the output active power when the micro-grid frequency steps with different droop controls.

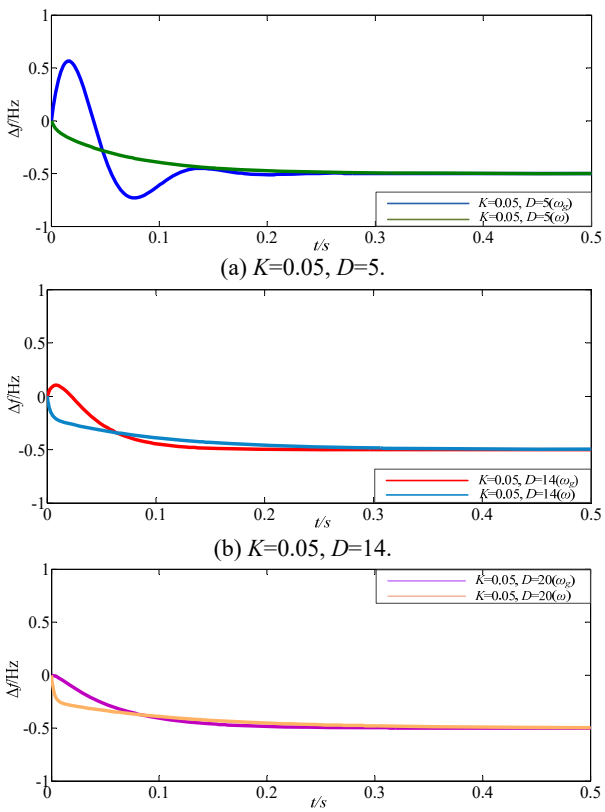

(a) K=0.05, D=5.

(b) K=0.05, D=14.

(c) K=0.05, D=20.

Fig. 9. Dynamic responses of the virtual rotor frequency when the micro-grid frequency steps with different droop controls.

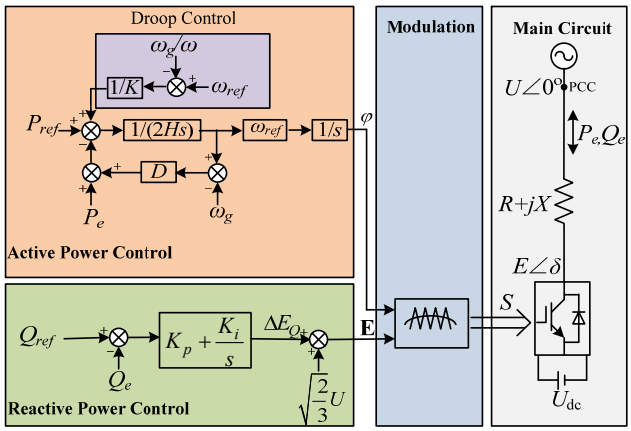

Fig. 10. Control diagram.

droop control methods can be switched between equation (5) and (6). **E** in Fig. 10 is shown in equation (24).

$$\frac{d\varphi}{dt}=\frac{d\delta}{dt}+\omega_g \tag{23}$$

$$\mathbf{E}=\begin{bmatrix}e_a\\e_b\\e_c\end{bmatrix}=\begin{bmatrix}E\sin\varphi\\E\sin(\varphi-2\pi/3)\\E\sin(\varphi+2\pi/3)\end{bmatrix} \tag{24}$$

where $\varphi=\int\omega\,dt$, $E=\sqrt{2/3}U+\Delta E_Q$.

VI. Simulation Results

The above mentioned ideas are verified by simulations in this section. The simulation system parameters of the VSM are the same as those of the theoretical analysis in Table I. Simulations are carried out in PSCAD/EMTDC 4.5, and the simulation results are presented without smoothing in order to be consistent with the theoretical analysis results. The switch frequency is set to 10 kHz and the solution time is set to 1μs.

A. Comparison between the Damping Factor and Droop Coefficient

The dynamic responses of the output active power and the rotor frequency in theoretical analysis and simulations are shown in Fig. 11 when the micro-grid frequency steps. The simulation results in Fig. 11 coincide well with the theoretical analysis results in Fig. 4. The simulation results with different values of K while D=5 are shown in Fig. 12. The output three phase currents of the VSM in Fig. 12(c) and (d) are obtained when K=0.05 and K=∞, respectively.

It can be concluded from Fig. 11 and Fig. 12 that the damping factor D has no influence on the steady value of ΔP_e. However, it influences the transient value of ΔP_e. K influences on both the steady value and transient value of ΔP_e. Both the damping factor D and the droop coefficient K influence the transient value of virtual rotor frequency Δf. However, the steady value of Δf is not influenced by D and K.

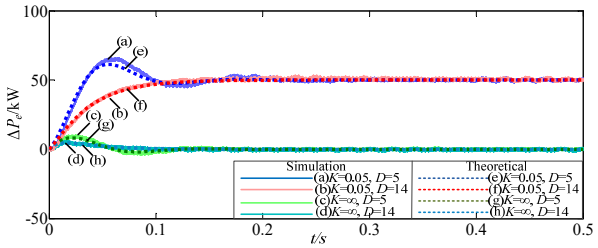

(a) Output active power with different K and D.

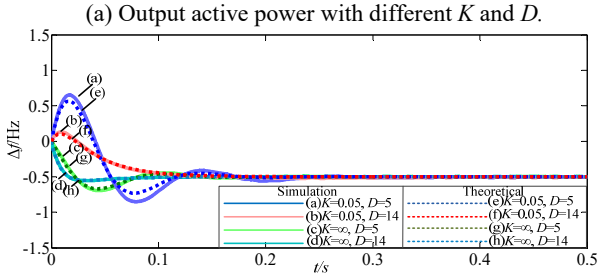

(b) Virtual rotor frequency with different values of K and D.

Fig. 11. Dynamic responses of the output active power and virtual rotor frequency when the micro-grid frequency steps.

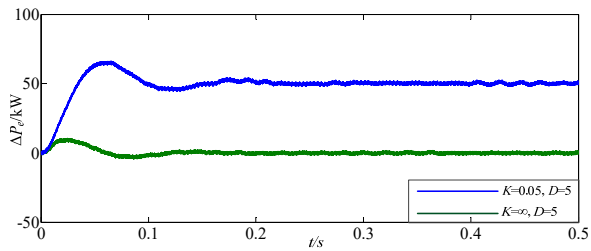

(a) Output active power with different values of K

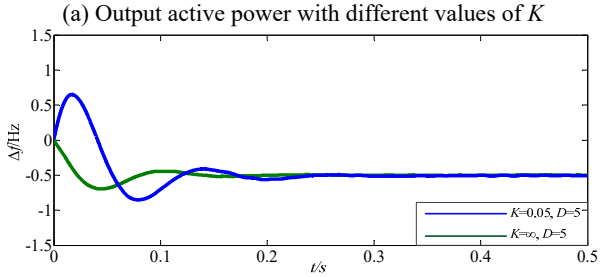

(b) Virtual rotor frequency with different values of K.

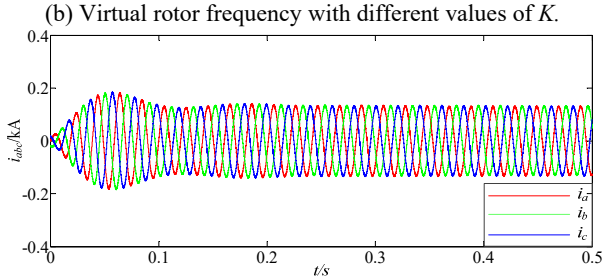

(c)Output currents when K=0.05, D=5.

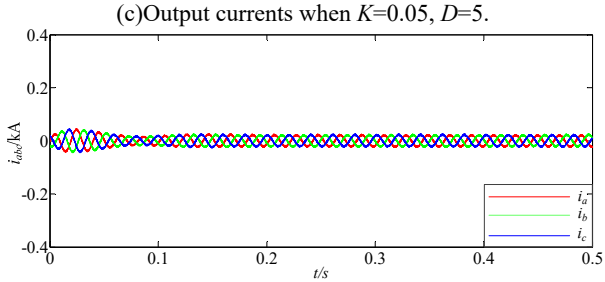

(d) Output currents when K=∞, D=5.

Fig. 12. Dynamic responses of the output active power and currents when the micro-grid frequency steps.

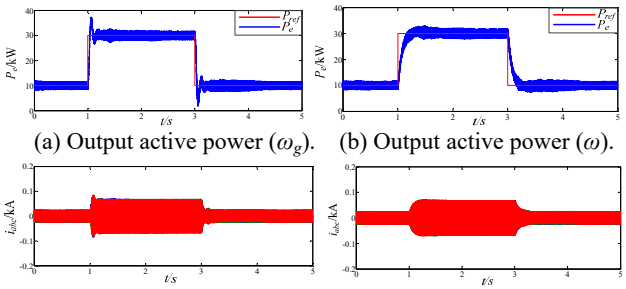

(a) Output active power (ω_g). (b) Output active power (ω).

(c) Output currents (ω_g). (d) Output currents (ω).

Fig. 13. Dynamic responses of the output active power and currents when P_{ref} steps with different droop controls (H=0.05s, D=5).

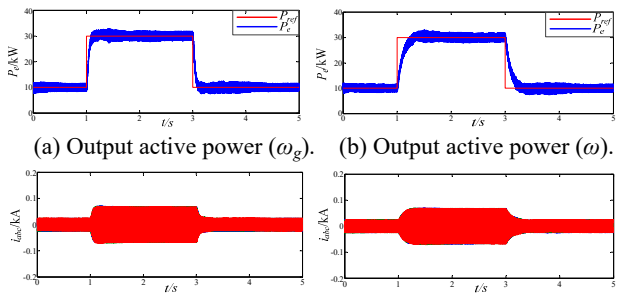

(a) Output active power (ω_g). (b) Output active power (ω).

(c) Output currents (ω_g). (d) Output currents (ω).

Fig. 14. Dynamic responses of the output active power and currents when P_{ref} steps with different droop controls (H=0.05s, D=14).

B. Comparison between Different Droop Control Methods

In order to illustrate the differences between the two droop control methods, simulations are carried out in this part when the reference of the output active power rises and the micro-grid frequency drops.

1) Reference of the Output Active Power Rises: Simulations in this part are started at t=0. The initial settings for P_{ref} is 10kW and that Q_{ref} is 0kVar. 30kW is applied to P_{ref} at t=1.0s and 10kW is then applied to P_{ref} at t=3.0s in Fig. 13 and Fig. 14. The theoretical analysis results in Fig. 7 are verified in this part. The simulation results in Fig. 13(a) and (c) as well as (b) and (d) are obtained by involving the droop control methods in equations (5) and equation (6). Equation (5) is in the under damping mode when compared with equation (6) in the over damping mode with the same control parameters. Equation (5) causes a large overshoot in the simulation. Fig. 14(a) and (c) as well as (b) and (d) are also obtained by involving the droop control methods in equations (5) and equation (6). Equations (5) and equation (6) are all in the over damping mode with same control parameters. However, equation (6) locates much worse in the over damping mode.

2) Micro-grid frequency drops

The dynamic responses of the output active power and the virtual rotor frequency in the theoretical analysis and simulations are shown in Fig. 15 and Fig. 16 when the micro-grid frequency steps. The simulation results coincide well with the theoretical analysis results in Fig. 8 and Fig. 9. The output active powers and currents with two different

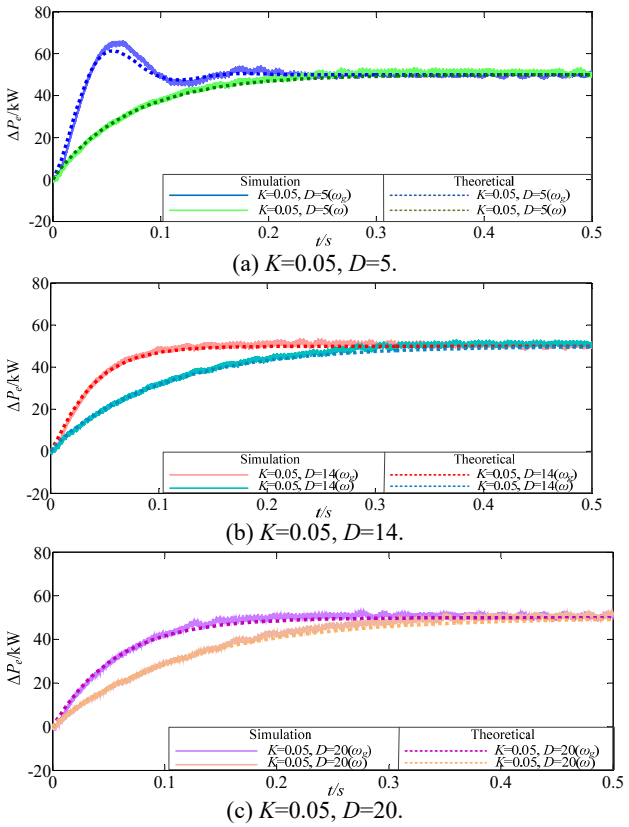

(a) K=0.05, D=5.

(b) K=0.05, D=14.

(c) K=0.05, D=20.

Fig. 15. Dynamic response of the output active power when the micro-grid frequency steps with different droop controls.

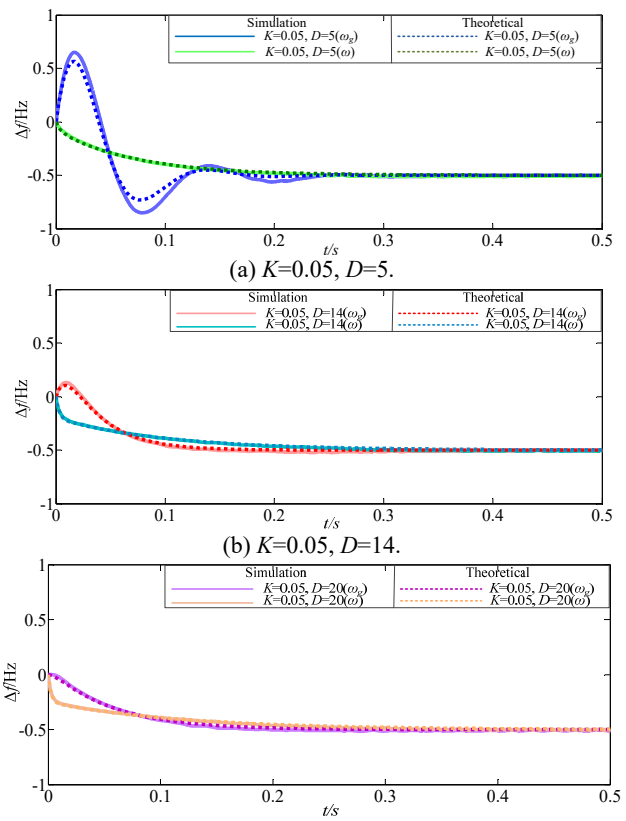

(a) K=0.05, D=5.

(b) K=0.05, D=14.

(c) K=0.05, D=20.

Fig. 16. Dynamic response of the virtual rotor frequency when the micro-grid frequency steps with different droop controls.

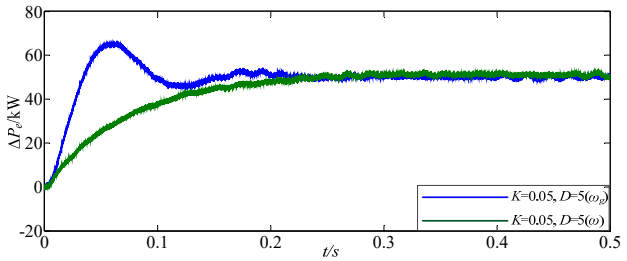

(a) Output active power with different droop controls.

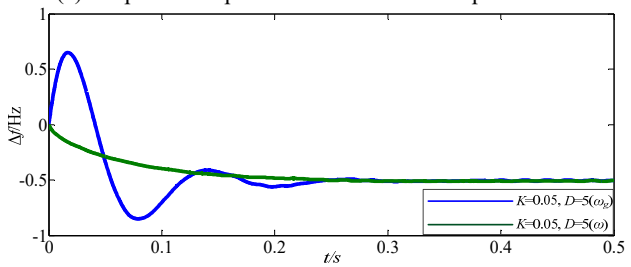

(b) Virtual rotor frequency with different droop controls.

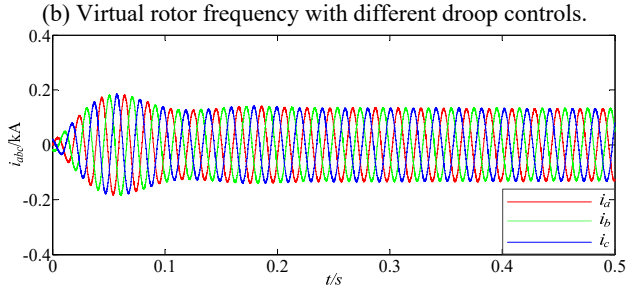

(c) Output currents (ω_g).

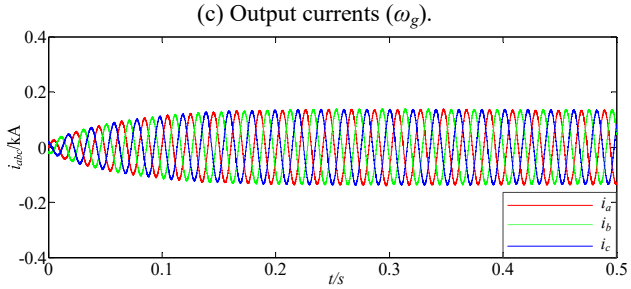

(d) Output currents (ω).

Fig. 17. Dynamic response of the output active powers and currents when the micro-grid frequency steps with different droop controls.

droop control methods are presented in Fig. 17 with different damping.

Simulations with different droop controls while K=0.05 are shown in Fig. 17. Fig. 17(c) and (d) are obtained from the droop control method equation (5) and (6).

The droop control method employing equation (6) can significantly increase the system damping when compared with equation (5) according to Fig. 16 and Fig. 17. It can be concluded that increasing of the damping factor D enhances the system stability from Fig. 16.

VII. Experimental Results

Experiments are also executed to verify the proposed idea. The experimental setup is presented in Fig. 18, and the experimental parameters are given in Table II.

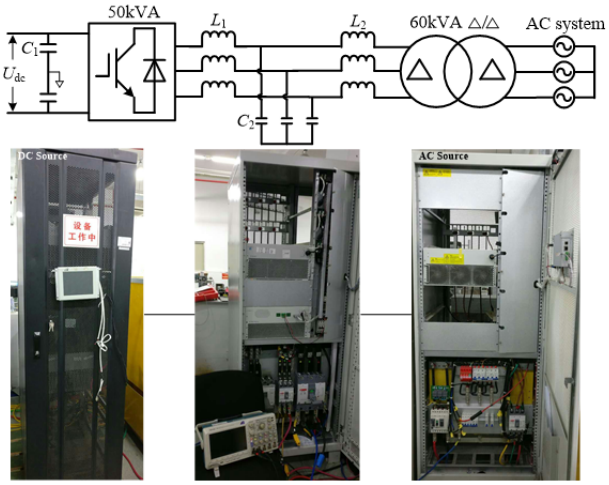

Fig. 18. Experimental setup.

TABLE II
Parameters of the Experimental Setup

Parameter	Value	Parameter	Value
S_n	50kVA	C_2	40μF
U_g(L-L)	380V	U_{dc}	700V
L_1	280μH	ω_{ref}	314rad/s
L_2	60μH	P_{ref}	10kW
C_1	470μF	H	0.05s

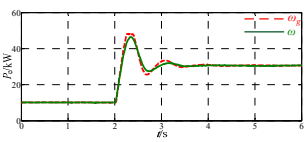

(a) Output active power.

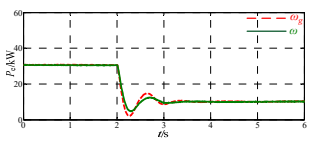

(b) Output active power.

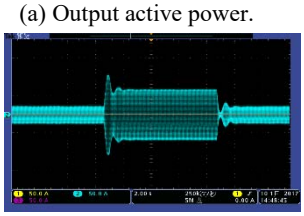

(c) Output phase current (ω_g).

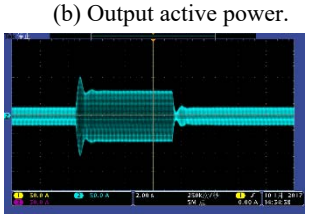

(d) Output phase current (ω).

Fig. 19. Experiments results when D=100.

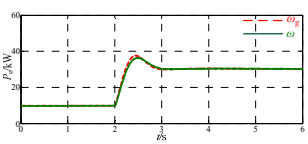

(a) Output active power.

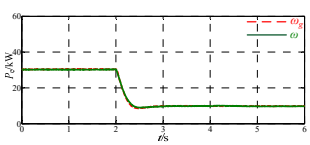

(b) Output active power.

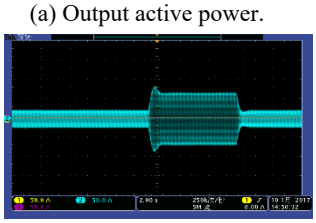

(c) Output phase current (ω_g).

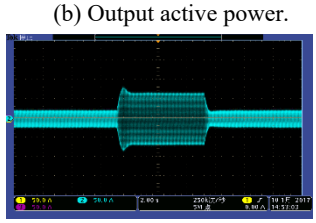

(d) Output phase current (ω).

Fig. 20. Experiments results when D=200.

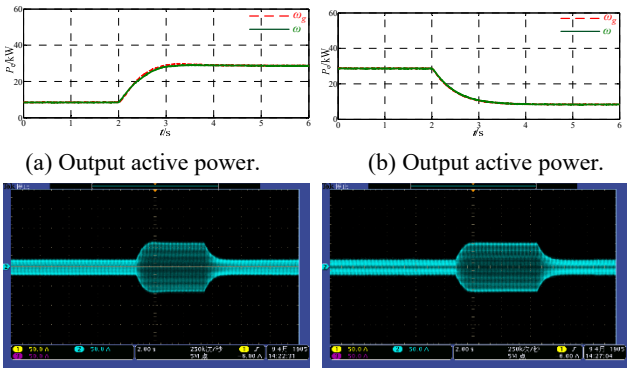

(a) Output active power. (b) Output active power.

(c) Output phase current (ω_g). (d) Output phase current (ω).

Fig. 21. Experiments results when D=550.

Experimental results when P_{ref} steps are presented in Fig. 19 to Fig. 21. The results when P_{ref} steps from 10kW to 30kW are shown in sub-graphs (a) in Fig. 19 to Fig. 21. The results when P_{ref} steps from 30kW to 10kW are shown in sub-graphs (b) in Fig. 19 to Fig. 21. The VSM output currents with the droop control in equation (5) when P_{ref} steps between 10kW and 30kW is also presented in sub-graph (c) in Fig. 19 to Fig. 21. In addition, the VSM output currents with the droop control in equation (6) are presented in sub-graphs (d) in Fig. 19 to Fig. 21

From the comparison results, it can be concluded that droop control method in equation (6) can increase the damping of a VSM system when compared with equation (5).

VIII. Conclusions

In this paper, a mathematical model of a VSM is built. The differences between the damping factor and the droop coefficient are studied. The dynamic responses of the VSM adopting different droop control methods are investigated in detail. Detailed simulation results verify the theoretical analysis. The main conclusions are summarized as follows

(1) The damping factor D is not always equivalent with the droop coefficient. The damping factor D has no influence on the steady state of ΔP_e. However, it has an influence on its transient value. K influences both the steady value and the transient of ΔP_e. Both the damping factor D and the droop coefficient K influence the transient of the virtual rotor frequency Δf. However, its steady state value is not influenced by D and K.

(2) The droop control method employing equation (6) can significantly increase the system damping when compared with equation (5). The VSM system with different droop control methods under the same parameters may locate in different damping modes.

(3) The droop control method employing equation (5)and(6) are all reasonable in the literature. However, equation (5) is suggested by this paper for the droop control method according to its physical meaning.

Acknowledgment

The authors would like to thank to Hui Fan, an engineer from Shenzhen Sinexcel Electric Co., Ltd., for his contribution to the experiments in this paper.

References

[1] China National Energy Administration-Development of China wind power industry in 2015-http://www.nea.gov.cn/2016-02/02/c_135066586.htm, February 2nd 2016.

[2] China National Energy Administration-Photovoltaic power generation statistical data of China in 2015-http://www.nea.gov.cn/2016-02/05/c_135076636.htm, February 5th 2016

[3] H. Bevrani, T. Ise, and Y. Miura, "Virtual synchronous generators: A survey and new perspectives," *International Journal of Electrical Power & Energy System*, No. 54, pp. 244-254, Jul. 2013.

[4] P. Tielens and D.V. Hertem, "The relevance of inertia in power system," *Renewable and Sustainable Energy Reviews*, No. 55, pp. 999-1009, Dec. 2015.

[5] T. Y. Zheng, L. J. Chen, T. Y. Chen, and S. Mei, "Review and prospect of virtual synchronous generator technologies," *Automation of Electric Power System*, Vol. 39, No. 21, pp. 165-175, Nov. 2015.

[6] H. P. Beck and R. Hesse, "Virtual synchronous machine," in *9th International Conference on Electric Power Quality and Utilization*, pp.1-6, 9-11, 2007.

[7] L. M. A. Torres L., L. A. C. Lopes, L. A Moran T., and J. R. Espinoza C., "Self-tuning virtual synchronous machine: A control strategy for energy storage systems to support dynamic frequency control," *IEEE Trans. Energy Convers.*, Vol. 29, No. 4, pp. 833-840, Dec. 2014.

[8] M. Benidris, S. Elsaiah, S. Sulaeman, and J. Mitra, "Transient stability of distributed generators in the presence of energy storage devices," in *North American Power Symposium*, pp.1-6, 2012.

[9] M. P. N. van Wesenbeeck, S. W. H. de Haan, P. Varela, and K. Visscher, "Grid tied converter with virtual kinetic storage," *IEEE PowerTech*, pp.1-7, 2009.

[10] Q. C. Zhong and G. Weiss, "Synchronverters: inverters that mimic synchronous generators," *IEEE Trans. Ind. Electron.*, Vol. 58, No. 4, pp. 1259-1267, Apr. 2011.

[11] Q. C. Zhong, P. L. Nguyen, Z. Y. Ma, and W. X. Sheng, "Self-synchronized synchronverters: Inverters without a dedicated synchronization unit," *IEEE Trans. Power Electron.*, Vol. 29, No. 2, pp. 617-630, Feb. 2014.

[12] H. Wu, X. B. Ruan, D. S. Yang, X. R. Chen, W. X. Zhao, Z. P. Lv, and Q. C. Zhong, "Small-signal modeling and parameters design for virtual synchronous generators," *IEEE Trans. Ind. Electron.*, Vol. 63, No. 7, pp. 4292-4303, Mar. 2016.

[13] Z. Zeng, W. H. Shao, L. Ran, and R. Li, "Mathematical model and strategic energy storage selection of virtual synchronous generator," *Automation of Electric Power System*, Vol. 39, No. 7, pp. 22-31, Jul. 2015.

[14] C. Cheng, H. Yang, Z. Zeng S.Q. Tang, and R.X Zhao, "Rotor inertia adaptive control method of VSG," *Automation of Electric Power System* , Vol. 39, No. 19, pp. 82-89, Oct. 2015.

[15] Z. P. Lv, W. X. Sheng, Q. C. Zhong, H. T. Liu, Z. Zeng, L.

Yang, and L. Liu, "Virtual synchronous generator and its applications in micro-grid, " *Proceedings of CSEE*, Vol. 34, No. 16, pp. 2591-2603, Jun. 2014.
[16] S. Wang, J. B. Hu, X. M. Yuan, and L. Sun, "On inertial dynamics of virtual synchronous controlled DFIG-based wind turbines," *IEEE Trans. Energy Convers.*, Vol. 30, No. 4, pp. 1691-1702, Dec. 2015.
[17] M. Y. Guan, W. L. Pan, J. Zhang, Q. R. Hao, J. Z. Cheng, and X. Zheng, "Synchronous generator emulation control strategy for voltage source converter (VSC) Stations," *IEEE Trans. Power Syst.*, Vol. 30, No. 6, pp. 3093-3101, Nov. 2015.
[18] Y. Du, J. M. Guerrero, L. C. Chang, J. H. Su, and M. Q. Mao, "Modeling, analysis, and design of a frequency-droop-based virtual synchronous generator for micro-grid applications," in *IEEE ECCE Asia*, pp.643-649, 2013.
[19] S. D'Arco and J.A. Suul, "Equivalence of virtual synchronous machines and frequency-droops for converter-based micro-grids," *IEEE Trans. Smart Grid*, Vol. 5, No. 1, pp. 394-395, Jan. 2014.
[20] J. H. Meng, Y. Wang, X. C. Shi, C. Fu, and P. Li, "Control strategy and parameter analysis of distributed inverters based on VSG," *Transactions of China Electrotechnical Society*, Vol. 29, No. 12, pp. 1-10, Dec. 2014.
[21] J. H. Meng, X. C. Shi, Y. Wang, C. Fu, and P. Li. "Control strategy of DER inverter for improving frequency stability of micro-grid," *Transactions of China Electrotechnical Society*, Vol. 30, No. 4, pp. 70-79, Feb. 2015.
[22] S. D'Arco and J.A. Suul, "Virtual synchronous machines – Classification of implementations and analysis of equivalence to droop controllers for micro-grids," in *IEEE PowerTech*, pp.1-7, 2013.
[23] S. D'Arco, J.A. Suul, and O.B. Fosso, "A virtual synchronous machine implementation for distributed control of power converters in Smart Grids," *Electric Power System Research*, No. 122, pp. 180-197, Feb. 2015.
[24] S. D'Arco, J.A. Suul and O.B. Fosso, "Small-signal modeling and parametric sensitivity of a virtual synchronous machine in islanded operation," *International Journal of Electric Power & Energy System*, No. 72, pp. 3-15, Mar. 2015.
[25] T. Shintai, Y. Miura, and T. Ise, "Oscillation damping of a distributed generator using a virtual synchronous generator," *IEEE Trans. Power Del.*, Vol. 29, No. 2, pp. 668-676, Apr. 2014.
[26] J. Alipoor, Y. Miura, and T. Ise, "Power system stabilization using virtual synchronous generator with alternating moment of inertia," *IEEE J. Trans. Emerg. Sel. Topics Power Electron.*, Vol. 3, No. 2, pp. 451-458, Jun. 2015.
[27] J. Liu, Y. Miura, and T. Ise, "Comparison of dynamic characteristics between virtual synchronous generator and droop control in inverter-based distributed generators," *IEEE Trans. Power Electron.*, Vol. 31, No. 5, pp. 3600-3611, Aug. 2015.
[28] J. Liu, Y. Miura, H. Bevrani, and T. Ise, "Enhanced virtual synchronous generator control for parallel inverters in micro-grids," *IEEE Trans. Smart Grid*, doi: 10.1109/TSG.2016.2521405, Feb. 2016.

Chang Yuan was born in Hunan, China, in 1981. He received his B.S. and Ph.D. degrees in Electrical Engineering from Xi'an Jiaotong University, Xi'an, China, in 2003 and 2010 respectively. He is presently working as a Lecturer in the North China Electric Power University, Beijing, China. His current research interests include power electronics applied to power system.

Chang Liu was born in Shandong, China in 1992. He received his B.S. degree from Shanghai University of Electric Power, Shanghai, China, in 2010. He is presently working towards his M.S. degree at the North China Electric Power University, Beijing, China. His current research interests include power electronics applied to power systems.

Xueyin Zhang was born in Sichuan, China in 1992. He received his B.S. degree from the North China Electric Power University, Beijing, China, in 2015. Currently, where he is presently working towards his Ph.D. degree. His current research interests include flexible power distribution technology and intelligent power conversion technology.

Tianyang Zhao was born in Inner Mongolia, China, in 1993. He received his B.S. degree from North China Electric Power University, Beijing, China, in 2011, where he is presently working towards his M.S. degree. His current research interests include power electronics applied to power systems.

Xiangning Xiao was born in Hunan, China, in 1953. He received his M.S. degree in Electrical Engineering from the North China Electric Power University, Beijing, China, in 1981. He was a Senior Research Scholar in the University of Bari, Bari, Italy, from October, 1991 to September, 1992. He is presently working as a Professor of Electrical Engineering at the North China Electric Power University. His current research interests include power electronics in power grids with new energy resources, power quality and its improvement in power systems, as well as power system sub-synchronous oscillations.

Niang Tang was born in Hunan, China, in 1984. He received his B.S. and M.S. degree in Electrical Engineering in 2006 and 2009 respectively, from the Changsha University of Science and Technology, Changsha, China. He received his Ph.D. degree in Electrical Engineering from the North China Electric Power University, Beijing, China, in 2013. He is presently working as an Engineer at the Electric Power Research Institute of Guangdong Power Grid Co., Ltd., Guangzhou, China. His current research interests include the power electronics and power quality.